International Journal of Rock Mechanics & Mining Sciences 70 (2014) 192–200

Contents lists available at ScienceDirect

International Journal of Rock Mechanics & Mining Sciences

journal homepage: www.elsevier.com/locate/ijrmms

Investigation and analysis of the rock burst mechanism induced within fault–pillars

Zhenlei Li [a,b], Linming Dou [a,b,*], Wu Cai [a,b], Guifeng Wang [a], Jiang He [b], Siyuan Gong [a], Yanlu Ding [a,b]

[a] State Key Laboratory of Coal Resources and Safe Mining, China University of Mining and Technology, Xuzhou 221116, China
[b] School of Mines, China University of Mining and Technology, Xuzhou 221116, China

ARTICLE INFO

Article history:
Received 6 July 2013
Received in revised form
1 February 2014
Accepted 17 March 2014
Available online 29 May 2014

Keywords:
Rock burst
Fault–pillar
Strata movement
Roof rotation
Pillar stress

ABSTRACT

An investigation is made of the characteristic strata movement and mechanism underlying fault–pillar induced rock bursts (FPIRBs) in order to mitigate rock burst damage in fault areas. A mechanical analysis of the fault–pillar model is established and roof rotation criteria is obtained. A formula is derived for the average static stress in the pillar through theoretical analysis, physical simulations, and engineering practice. The results show that when a coalface approaches a fault area, two or more roof strata simultaneously fracture in the fault area, leading to an increase in the dynamic and static stresses in the pillar. The most important factors affecting FPIRB are the static stress in the pillar and the dynamic stress induced by fault slides. The roof block rotates more easily when the pillar width is smaller, the roof thickness larger, and the roof subsidence smaller. The average static stress in the pillar increases with decreasing pillar width and/or increasing roof fracture length. The stress is greater if there is a voussoir beam structure, in which case the stress is directly proportional to the squared length of the fractured roof, and inversely proportional to the squared width of the pillar just before rotation occurs. After rotation, it is directly proportional to the roof fracture length and inversely proportional to the pillar width. Based on the FPIRB mechanism and analysis of the mechanical model, six methods of FPIRB prevention are proposed. Also, we find that FPIRB occurrence can be effectively reduced by the use of de-stress blasting and large diameter drilling.

1. Introduction

Rock bursts are currently one of the severest threats to safe coal mining, especially in China. Their results can be disastrous and can result in tremendous numbers of casualties and socioeconomic loss. For example, a rock burst in the Sunjiawan Coalmine in 2005 caused 214 deaths and left 30 people injured. Six years later, on 3 November 2011, a rock burst due to a fault in the Qianqiu Coalmine caused the death of 10 people and left 75 people trapped underground.

As mining depth is increasing year by year, rock bursts are happening more frequently [1,2]. When mining activities approach high stress zones (like faults, folds, and residual pillar areas, *etc.*), rock bursts or tremors with high energy are more likely to happen [1–7]. As a result, rock bursts around faults and pillar areas and their mechanisms have been studied and analyzed using various methods by scholars around the world [8–16]. However, no unanimous viewpoint has been reached on rock bursts because of their complicated formation mechanism. Furthermore, fault–pillars have rarely been taken into consideration when studying the fault activity mechanisms that induce rock bursts. Consequently, the importance of fault–pillars has been overlooked.

In this paper, the importance of fault–pillars is investigated with regard to rock bursts. A mechanical model of a fault–pillar is established and analyzed to reveal new insights into the in-depth mechanism underlying FPIRBs. Based on the elucidated mechanism and mechanical model analysis, corresponding burst prevention methods are proposed and their validity is confirmed using practical tests.

2. The FPIRB mechanism

2.1. Rock bursts induced by superposition of static and dynamic stresses

A rock burst may occur when the total stress (due to the superposition of the static stress in the coal and the dynamic stress induced by tremors) reaches a certain critical stress level [17]. The stress criterion for rock burst occurrence can be expressed in the form

$$\sigma_j + \sigma_d > [\sigma_b], \tag{1}$$

* Corresponding author at: State Key Laboratory of Coal Resources and Safe Mining, China University of Mining and Technology, Xuzhou, Jiangsu 221116, China. Tel.: +86 13952261972.
E-mail addresses: cumtzhenleili@163.com (Z. Li), lmdou@cumt.edu.cn (L. Dou).

http://dx.doi.org/10.1016/j.ijrmms.2014.03.014
1365-1609/

where σ_j is the static stress in the coal, σ_d is the dynamic stress induced by the tremor, and $[\sigma_b]$ is the critical stress required for rock burst formation. Eq. (1) indicates that the interaction of σ_j and σ_d can lead to a rock burst. Hence, it is possible to control rock bursts by reducing σ_j or σ_d.

2.2. Strata movement characteristics

Fracturing in the overlying strata is in terms of the "O–X" structure and coal mass is subject to abutment stress during coal extraction [18,19]. When the coalface approaches the fault area, the abutment stress increases gradually or suddenly and rock burst accidents can easily occur [4,10].

A physical simulation experiment was performed to compare normal mining and the situation in which the coalface approaches the fault area. The results, shown in Fig. 1, allow the differences in strata movement to be figured out and the reasons for rock bursts to be investigated. Under normal mining conditions, the roof strata fracture occurs one by one, not simultaneously, from bottom to top. Almost none of the fracture surfaces lie in the same straight line. In fact, nearly all the fracture surfaces lie behind the coalface, leaving roof strata hanging behind in the gob area. On the whole, the coal ahead of the coalface is affected by the lead abutment pressure. On the other hand, when the coalface approaches a fault area, two or more roof strata fracture simultaneously in the fault area, leading to a decrease in the stress in the fault area. As a result, the weight of the fractured roof layers is imposed on the fault–pillar. As the pillar sizes decrease, the stress within the pillars rises.

2.3. The rock burst mechanism

The physico-mechanical properties and stress distribution in the coal-rock mass are discontinuous in the fault area [7,10,14]. Thus, when mining activities approach the fault area, fault–pillars are formed [11]. In such cases, pillar failure or fault slides can induce rock bursts. This is the root cause of the FPIRB phenomenon. According to main factors involved, FPIRB can be divided into rock bursts that are fault slide induced, pillar failure induced, and those induced by the interaction between fault slides and pillar failure [corresponding to (a), (b), and (c) in Fig. 2, respectively]. These three cases are discussed separately, as follows:

2.3.1. Fault slide induced rock bursts

When mining activities are far away from the fault area, the influence of the fault on the stress distribution in the coal–rock mass is small. As a result, the stress in the coal–rock mass is the

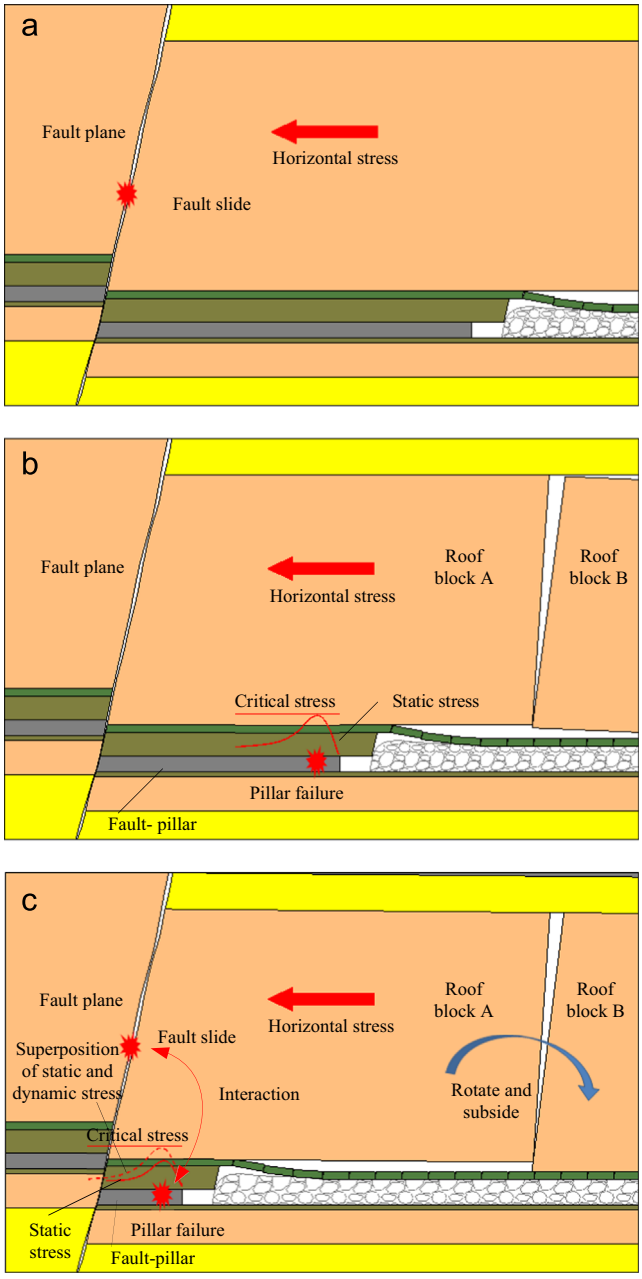

Fig. 2. Sketches showing the mechanism associated with FPIRB.

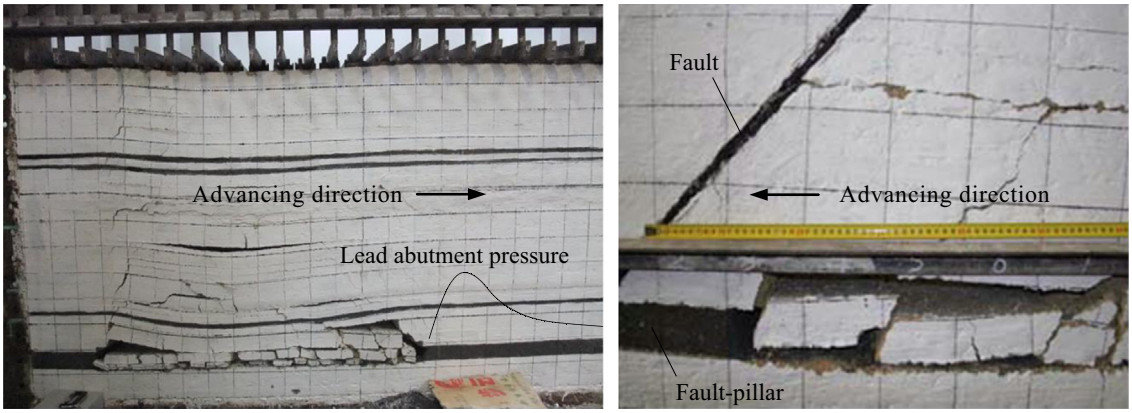

Fig. 1. Strata movement characteristics probed using physical simulation.

same as that in normal mining. Under these circumstances, if a sudden slide occurs in the fault area, a large amount of energy may be released, and a rock burst may result. Fault sliding is the main factor affecting bursts in this process as it induces dynamic stress and releases energy; see Fig. 2(a).

2.3.2. Pillar failure induced rock bursts

When mining activities approach the fault area, they will interact with the fault. The overlying strata will fracture, rotate, subside, and then collapse. This results in the lowering of normal stress and frictional supporting stress around the fault plane and therefore increases the weight of the overlying strata imposed on the fault–pillar. The smaller the pillar size, the larger will be the static stress within the pillar. When the stress reaches a critical value, a rock burst will occur and the part of the pillar adjacent to gob area will break first. A high static stress in the pillar is the main burst factor in this process; see Fig. 2(b).

2.3.3. Rock bursts induced by the interaction of a fault slide and pillar failure

In addition to the above two cases, there must also be another case. In this case, static stress in the pillar has not quite reached the critical stress and a fault slide alone would not be sufficient to induce a rock burst. However, the simultaneous action of the two factors can lead to a rock burst. A fault slide causes a tremor, making the total stress from the superposition of the two different stresses meet the stress criterion for rock burst. Then, the pillar bumps and fails, causing a burst disturbance which in turn further promotes the fault slide process. Here, energy is not only released by the fault slide but also from the energy accumulated in the pillar. The interaction of a fault slide and pillar failure is the main burst factor here; see Fig. 2(c).

From the above analysis, it can be concluded that if mining activities are far away from the fault, the main burst factor is the fault slide induced dynamic stress and the burst energy comes from the fault accumulated energy. Otherwise, the main burst factors are the fault slide induced dynamic stress and high static stress in the pillar. In this case, the source of the burst energy is the energy accumulated in both the fault and the pillar.

3. Mechanical analysis of a fault–pillar

3.1. Mechanical analysis model

According to voussoir beam theory [2,20–25], compressive and shear stresses form in the fault area due to the horizontal thrust. A hard and thick roof stratum has a great influence on coal breakage because a high dynamic stress load is imposed on the coal mass when it fractures [26–28]. In this paper, we select a hard/thick roof stratum near the coal and simplify it as a beam to establish the mechanical analysis model, as shown in Fig. 3. In the figure, A and B are fractured roof blocks; M is the contact point between A and B; L is the roof fracture length; L_1 is the width of the fault–pillar ($L_1 \le L$); H is the thickness of the roof; ρ is the density of the roof; θ is the angle of the fault plane in the vertical direction; s is the subsidence of roof block B; p is the uniform stress load caused by the overlying strata; σ is the uniform compressive stress in the fault area; τ is the uniform shear stress in the fault area; $f(l_1)$ is the static stress distribution function within the fault–pillar; T is the horizontal thrust between roof blocks A and B; R is the friction between A and B; and φ is the friction angle of the fault.

The mechanical equilibrium of roof block A requires:

$$\begin{aligned}
&\sigma H-\tau H\ \tan\theta-T=0,\\
&\int_0^{L_1} f(l_1)dl_1-\tau H-R-\sigma H\ \tan\theta-p(L-H\ \tan\theta)-\rho gH(L-\tfrac{1}{2}H\ \tan\theta)=0,\\
&\int_0^{L_1} f(l_1)l_1dl_1-RL-\tfrac{\sigma H^2}{2\cos^2\theta}-\tfrac{1}{3}\rho gH^3\tan^2\theta-\tfrac{1}{2}(p+\rho gH)(L^2-H^2\tan^2\theta)=0,\\
&\tau\le\sigma\ \tan\varphi.
\end{aligned} \tag{2}$$

The horizontal thrust T and friction R can be expressed as [2,20,21]

$$T=\frac{L}{2(H-s)}Q_B, \tag{3}$$

$$R=Q_B, \tag{4}$$

where Q_B is the stress load due to roof block B and its overlying strata, which is called 'load B' in this paper for the sake of brevity.

By introducing a parameter q representing the stress load per unit length (also referred to as load density), Q_B can be written as

$$Q_B=(p+\rho gH)L=qL. \tag{5}$$

For a specific coalface, the parameters L, L_1, H, θ, s, p, ρ, and φ can be obtained by physical measurement. If the form of $f(l_1)$ is confirmed or assumed, the unknown variables σ and τ can be found from Eq. (2). The degree of the burst danger can be evaluated using the value of σ [17].

In order to solve engineering problems, we assume $f(l_1)$ has a uniform distribution. This allows us to obtain the average static stress f_{av} in the fault–pillar. In this case, $f(l_1)$ is equivalent to f_{av} (i.e. $f(l_1)=f_{av}$). We also define a coefficient K ($K>1$) such that the maximum stress is Kf_{av} (i.e. K times the average stress f_{av}). The coefficient K can be acquired from a combination of theoretical calculation and mine pressure measurement. In this case, the solutions to Eq. (2) are given by

$$\begin{aligned}
f_{av}&=\frac{1}{L_1(L_1-H\ \tan\theta)}[2RL+H(T-R\ \tan\theta)\\
&\quad+qL(L-H\ \tan\theta)+\frac{1}{6}\rho gH^3\tan^2\theta],\\
\sigma&=\frac{\cos^2\theta}{H(L_1-H\ \tan\theta)}[R(2L-L_1)\tan\theta+TL_1\\
&\quad+q\ \tan\theta(L-H\ \tan\theta)(L+H\ \tan\theta-L_1)\\
&\quad-\frac{1}{6}\rho gH^2\tan^2\theta(3L_1-4H\ \tan\theta)],\\
\tau&=\frac{\cos^2\theta}{H(L_1-H\ \tan\theta)}[R(2L-L_1)+T\left(\frac{H}{\cos^2\theta}-L_1\ \tan\theta\right)\\
&\quad+q(L-H\ \tan\theta)(L+H\ \tan\theta-L_1)\\
&\quad-\frac{1}{6}\rho gH^2\ \tan\theta(3L_1-4H\ \tan\theta).
\end{aligned} \tag{6}$$

3.2. Discussion of the model

The voussoir beam structure cannot be maintained in the following two cases [2]: (1) roof block B slides down ('slide instability'), and (2) contact point M between roof blocks A and B breaks, leading to further rotation and subsidence of roof block B ('deformation instability'). Hence, the conditions necessary for the existence of the voussoir beam structure are deduced to be

$$L>\frac{2(H-s)}{\tan(\varphi_1-\theta_1)} \tag{7}$$

and

$$s<H\left[1-\sqrt{\frac{1}{3nK\overline{K}}}\right], \tag{8}$$

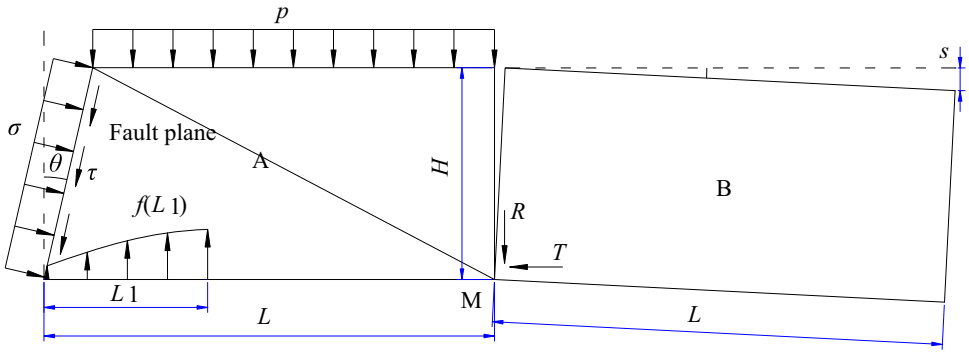

Fig. 3. The model used in the mechanical analysis of the fault–pillar.

where φ_1 is the friction angle between the roof blocks, θ_1 is the angle of the fracture surface in the vertical direction, n is the ratio of the rock's tensile and compressive strengths, and $\overline{K}$ is the ratio of squeezing strength of the contact point and the rock's compressive strength. The value of K is in the range ½ to 1/3, depending on the form of support for the beam ends (simple supported beam or clamped–clamped beam, *etc.*).

It may be concluded that there are two cases to be considered in the model. Either the voussoir beam structure is formed and maintained or the voussoir beam structure does not exist.

Assuming $\theta=0^\circ$, the stress load Q_A due to roof block A and its overlying strata (again simply referred to as 'load A' here) will be equivalent to Q_B (i.e. $Q_A=Q_B$). The two aforementioned cases are discussed separately, as follows:

3.2.1. *A voussoir beam structure is maintained*

In this case, roof block A will rotate when the pillar width L_1 becomes small enough. The rotation criterion is deduced to be

$$\frac{7H-6s}{L_1}-\frac{4(H-s)}{L}> \tan\varphi. \tag{9}$$

According to Eq. (9), rotation of roof block A is decided by the roof block sizes L and H, the pillar width L_1, the roof block subsidence s, and the fault friction angle φ, rather than the stress in the pillar. For a specific fault, φ has a constant value. Generally, the following two equations are valid [2]: $\varphi\le 38^\circ$–45° and $\tan\varphi\le 0.8$–1. Hence, it is inevitable that roof block A will rotate when the pillar width L_1 is small enough.

Before block A rotates, load A and load B are supported jointly by the fault friction τH and the fault–pillar. Hence, the average stress is deduced to be

$$f_{av}=q\frac{L^2}{L_1^2}\frac{7-6i}{2(1-i)}, \tag{10}$$

where i is the ratio of s and H.

Eq. (10) indicates that the average static stress in the pillar is directly proportional to the square of the length of the fractured roof, and inversely proportional to the square of the width of the pillar.

After block A rotates, there will be some changes arising in the mechanical model. This has been confirmed by other researchers [2]. The changes of interest are that when the contact point M moves up, friction R becomes zero, and the stresses σ and τ cease to exist. As a result, the pillar alone supports load A. However, the horizontal thrust T is the same as before. In this case, the average stress is deduced to be

$$f_{av}=q\frac{L}{L_1}. \tag{11}$$

Eq. (11) indicates that the average static stress in the pillar is directly proportional to the roof fracture length and inversely proportional to the pillar width.

3.2.2. *A voussoir beam structure does not exist*

In this case, roof block B has collapsed. Thus, there is no force in effect between blocks A and B. In addition, A will inevitably rotate since it has been assumed that $f(l_1)$ has a simple uniform distribution. When the hanging end of A touches the collapsed strata, the rotation process stops. As a result, the pillar together with the collapsed strata supports load A. The average stress is deduced to be

$$f_{av}=q\frac{L^2}{(2L-L_1)L_1}. \tag{12}$$

The mechanical model of the fault–pillar presented here is a practical and useful way of calculating the static stress in the fault–pillar. If the actual static stress distribution in the fault–pillar and related parameters can be determined, the static stress in the pillar can be evaluated exactly and used to evaluate the degree of the burst danger more accurately according to the derivation process of the model.

3.3. *Variation laws for the key parameters in the model*

In light of the form of Eq. (10), we introduce a new variable $f(i)$, defined by (see Fig. 4)

$$f(i)=\frac{7-6i}{2(1-i)}. \tag{13}$$

when $i<0.5$, $f(i)$ is approximately proportional to i. However, when $i>0.7$, $f(i)$ increases very rapidly as i increases (see Fig. 4). According to Eq. (8), deformation instability rarely arises in the voussoir beam structure when $i<0.68$. Thus, generally, $3.5<f(i)<4.56$.

Considering the form of Eq. (9), we introduce another new variable $f(i,L_1)$, given by

$$f(i,L_1)=\frac{7H-6s}{L_1}-\frac{4(H-s)}{L}. \tag{14}$$

Assuming the roof fracture length is $L=20$ m, the relationship between $f(i,L_1)$ and parameters i, H and L_1 can be visualized, as shown in Fig. 5. From the figure, it can be concluded that for any given values of the parameters L, i, and H, the roof block A will more easily rotate when the pillar width is smaller. Also, rotation is inevitable when the pillar width decreases to a certain value. If the parameters L, L_1, and H are given, then A will be more likely to rotate for smaller values of i. This means that the smaller the subsidence of roof block B (i.e. the value of s), the easier it is for A

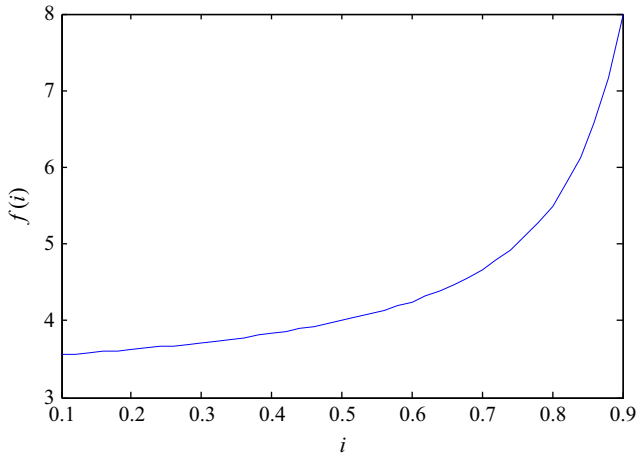

Fig. 4. Curve showing the relationship between $f(i)$ and i.

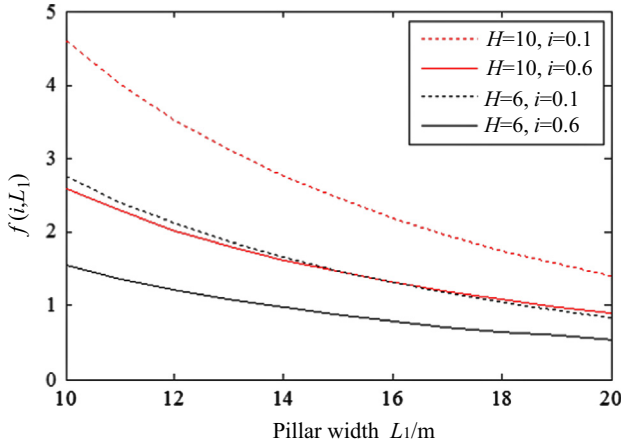

Fig. 5. Criteria for rotation of roof block A.

to rotate. If the parameters L, L_1, and i are given, then A is more likely to rotate at larger roof thicknesses H.

Assuming the roof thickness is $H=20$ m and $\tan\varphi=1$, the relationship between the average static stress f_{av} and the parameters i, L and L_1 can be visualized, as shown in Fig. 6. In the figure, note that the ordinate values of f_{av} are multiples of the load density q.

Fig. 6 shows that the average static stress f_{av} increases as the pillar width L_1 decreases. For a given value of L_1, f_{av} increases as the roof fracture length L increases. For example, when $L_1=2$ m, f_{av} in Figs. 6(a) ($L=20$ m) and 6(b) ($L=30$ m) is $10q$ and $15q$, respectively. Also, for a certain L_1 value, f_{av} with a voussoir beam structure is higher than that without a voussoir beam structure. With a voussoir beam structure, roof block A will inevitably rotate as L_1 decreases. The average static stress is inversely proportional to the square of the width of the pillar (L_1^2) just before rotating and inversely proportional to the pillar width L_1 after rotating. There is a sudden drop in the average static stress when roof block A rotates. For given L_1 and L values, the smaller the value of i, the easier it is for A to rotate. Before rotating, f_{av} decreases accordingly as i decreases. After rotating, f_{av} is not affected by i.

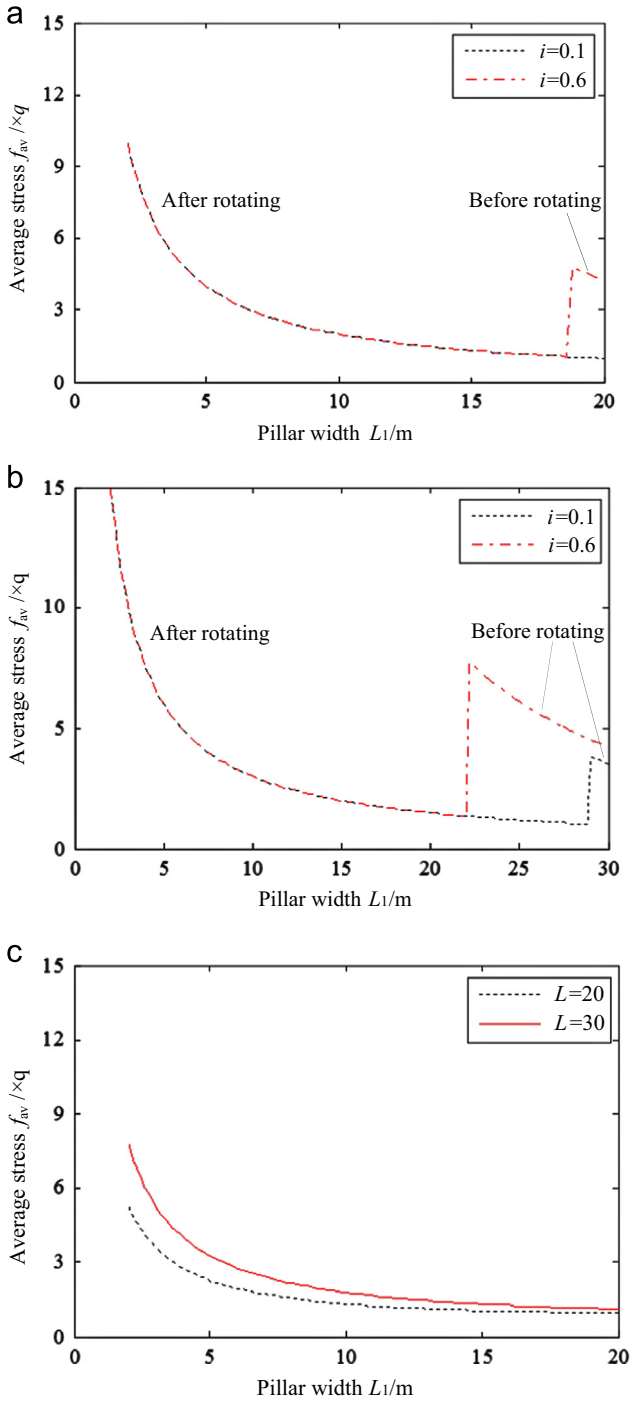

Fig. 6. Curves showing the relationship between the average static stress and pillar width when there is a voussoir structure and (a) $L=20$ m and (b) $L=30$ m. In (c), the equivalent curves are shown when a voussoir beam structure is absent.

4. Controlling FPIRBs

Based on the study of the FPIRB mechanism and analysis of the mechanical model, it can be concluded that FPIRB disasters can be made less likely to occur by reducing the static stress in the pillar, the fault slide induced dynamic stress, and the energy accumulated in the pillar. Detailed methods of accomplishing this are as follows:

(1) Pre-split the roof to reduce roof fracture length. Consequently, loads A and B would both be reduced and slide instability is prompted to arise in a voussoir beam structure. This leads to only load A being imposed on the fault–pillar.
(2) Fill the gob area behind the coalface. Thus, roof subsidence is decreased which prompts roof block A to rotate at a larger

pillar width. This results in a lowering of the static stress in the pillar.

(3) Make the coalface oblique to the fault to avoid the pillar width becoming smaller integrally.

(4) Loosen and crack the roof. This reduces the hanging length of the roof in the gob and prompts the roof strata to collapse timely after mining. Consequently, static stress in the pillar does not grow as significantly as the pillar width decreases.

(5) Control mining intensity to reduce the disturbance to the fault caused by mining activities so that the possibility of a fault slide is reduced.

(6) Loosen and crack the coal mass ahead of the coalface. This reduces the burst tendency, compressive strength, and energy accumulation of the coal mass so that the critical stress for rock burst occurrence is raised and FPIRB becomes more difficult to happen.

5. Practical experiences of FPIRBs

5.1. Site details

The selected coalface is in Yuejin Coalmine of Henan Dayou Energy Company Limited, China. Longwall technology was adopted for the underground mining of coal seam 2–1, whose thickness varies from 8.4 to 13.2 m. The length of longwall panel 25110 is 865 m and its width is 191 m. Mining in this panel began on 17 July 2010 and was completed on 7 January 2013. The entire thickness of the coal seam in this panel was extracted using a fully mechanized longwall face with caving. Panel 25090, whose upper slice was extracted through slice mining, is situated next to panel 25110 in the north (see Fig. 7). In the south, lies fault 16 and the distance between panel 25110 and the fault varies from 75 to 230 m. Three small faults were situated in the middle of the panel. The eastern and western parts of the area next to panel 25110 were not extracted.

The cover depth of the coal seam in the selected panel varied from 950 to 1000 m and the inclination of the coal seam varied from 10° to 15° in the northeastern direction. The upwards roof strata consisted of mudstone (18 m), coal seam 1–2 (1.5 m), mudstone (4 m), and sandstone (190 m). The downwards floor strata were mudstone (4 m) and sandstone (26 m).

With a fault throw varying from 50 to 500 m and a horizontal fault offset varying from 120 to 1080 m, fault 16 extends for about 45 km. The inclination of the fault is 75° in the shallow area and varies from 15° to 35° in the deep area.

5.2. Installed seismic system

Poland ARAMIS M/E system was installed in Yuejin Coalmine. The system, which is based on SPI-70 seismometers (type of sensors) in SN/DTSS transmission stations, is used to locate rock bursts, determine the energy of bursts and assess rock burst hazards. There are 16 component channels with one SP/DTSS cassette in the system. The system uses intrinsically safe data transmission, centrally supplied from the surface, which enables to transmit 1-, 2- or 3-axial velocity movements (*X*, *Y*, *Z*). The sampling of signals is performed by means of 24-bit Sigma Delta converters, providing high dynamics of conversion and recording. Sixteen stations were installed in the system, as shown in Fig. 8. The stations were distributed spatially all around the mine to monitor microseismic events of the whole coalmine, while the main target is longwall panel 25110. 12 of them were fixed in gateways and entries and 4 of them (13, 14, 15 and 16 in Fig. 8) were moving parallel to coal face advance.

5.3. Rock burst occurrence

A microseismic event contains spatial location and energy release. Spatial locations can reveal the processes of initiation, development and expansion of micro-fractures inside the coal–rock mass [29]. These processes may develop to a rock burst, whose essence is energy release [30]. Hence, a study of microseismic events is of vital importance for the reveal of rock burst mechanism.

Influenced by the roof strata and the faults, rock bursts occurred 20 times in panel 25110 (7 times during gateway tunneling and 13 times as the coalface advanced). The rock burst events were monitored and located by Poland ARAMIS M/E system installed in the Coalmine (their locations are indicated in Fig. 7). It can be seen from Fig. 7 that the burst sources are mainly distributed in the area around the head gate, fault 16, and the smaller faults. With the advancement of the tunneling face (coalface), the distance between fault 16 and the tunneling face (coalface) became smaller (larger), and the burst sources gradually approached (departed from) the head gate and fault 16. When the longwall face approached the small faults, rock bursts happened

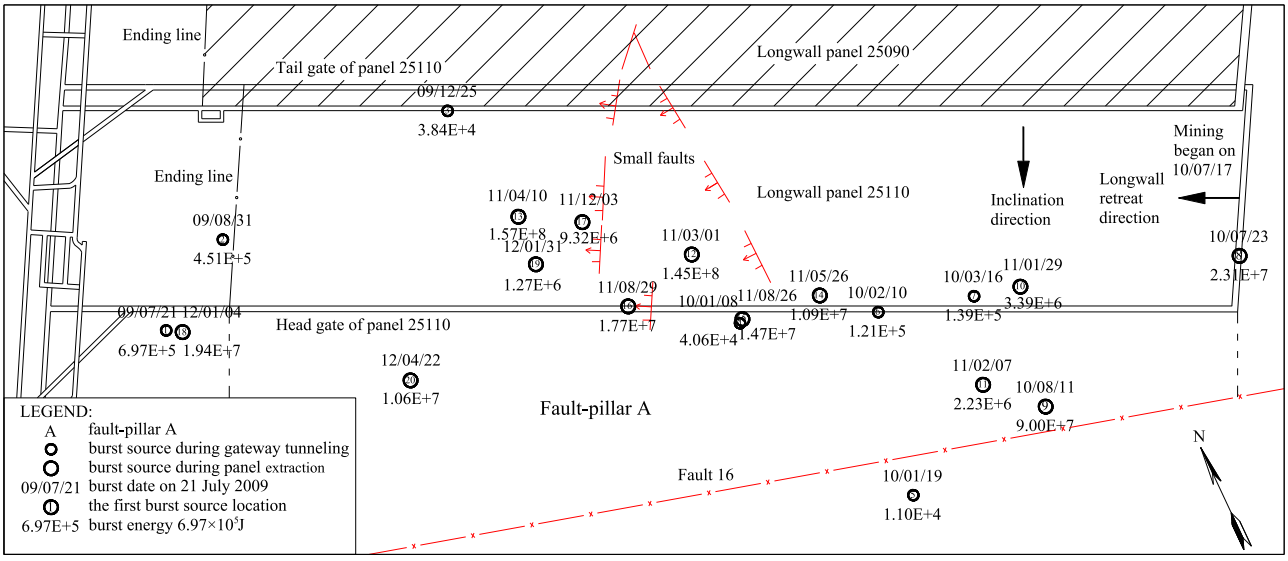

Fig. 7. Gateway layout and burst source distribution in a mining panel.

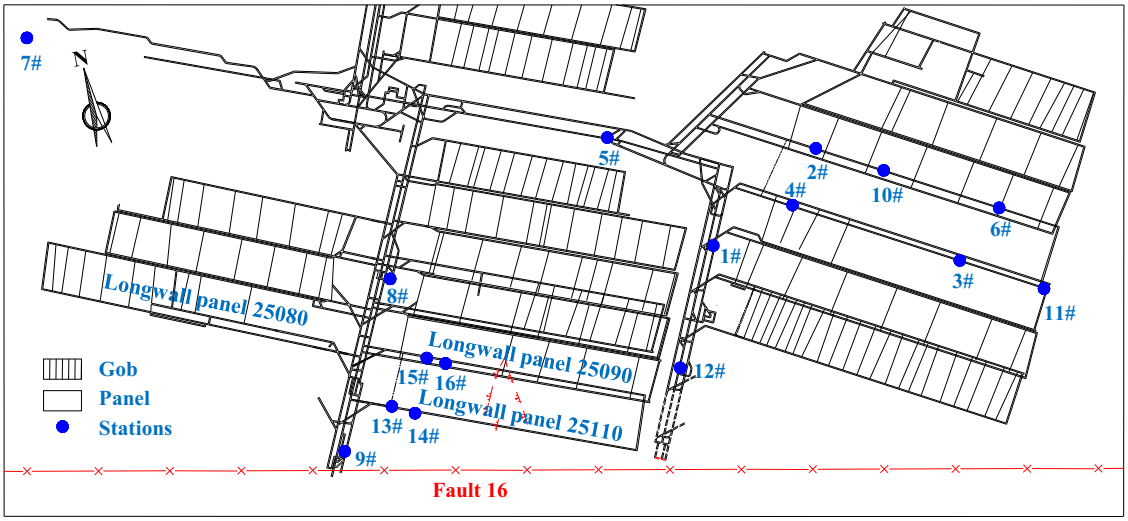

Fig. 8. Distribution of stations of ARAMIS M/E system installed in Yuejin Coalmine.

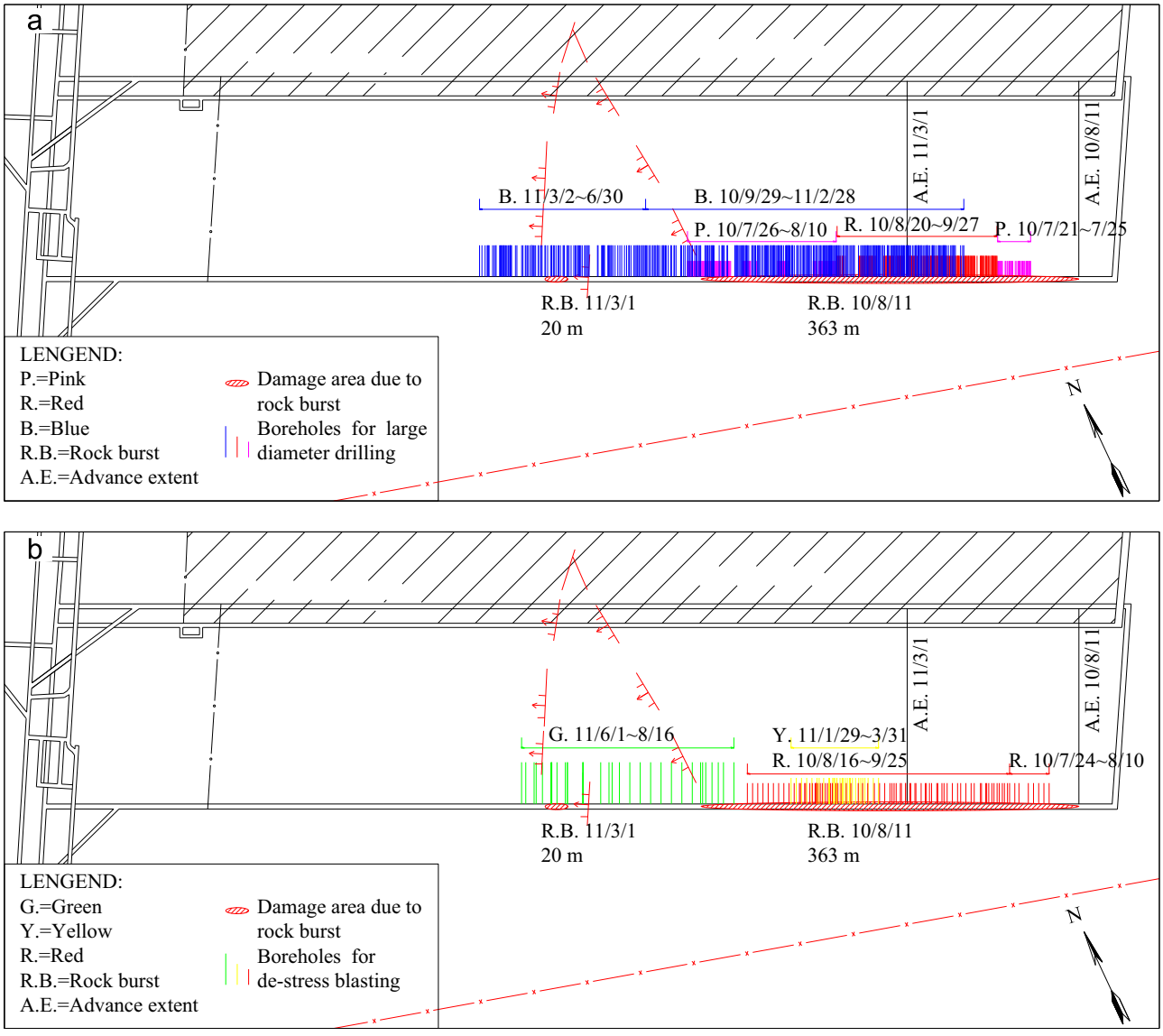

Fig. 9. Boreholes layout for (a) large diameter drilling and (b) de-stress blasting.(For interpretation of the references to color in this figure, the reader is referred to the web version of this article.)

more frequently and the energy released became greater. Burst energies during coalface advancement (10^6–10^8 J) were much greater than those during gateway tunneling (10^4–10^5 J).

The distribution characteristics of the burst sources observed above and shown in Fig. 7 can be explained with the help of the FPIRB mechanism discussed earlier. The scale of the strata movement during panel extraction was larger than that during gateway tunneling, which induced a stronger disturbance effect on the fault and larger dynamic and static stress loads on the pillar. As a result, the burst frequency and energy during panel extraction was higher than that during gateway tunneling. With the advancement of the coalface, the width of the fault–pillar (A in Fig. 7) increased from 75 to 230 m, and the pillar width between the small faults and the coalface gradually decreased and eventually disappeared. As inferred in Section 3, pillar width is one of the main factors affecting the static stress. Furthermore, the disturbance effect on the fault became more severe when the pillar width decreased. Hence, the burst frequency and energy became greater as the longwall face approached the small faults.

Table 1
Borehole parameters for large diameter drilling.

Boreholes for large diameter drilling	Borehole length (m)	Borehole diameter (mm)	Date
Pink ones	15	75	21 July to 10 August 2010
Red ones	20	75	20 August to 27 September 2010
Blue ones	30	100	29 September 2010 to 30 June 2011

Table 2
Borehole parameters for de-stress blasting.

Boreholes for de-stress blasting	Borehole length (m)	Explosives' weight (kg)	Date
Red ones	20	10.8	24 July to 25 September 2010
Yellow ones	25	18	29 January to 31 March 2011
Green ones	40	36	1 June to 16 August 2011

5.4. Preventative measures and their effects

Large diameter drilling and de-stress blasting can loosen and crack the coal mass, reduce the static stress, and partially release the energy accumulated in the coal mass. These two methods were adopted for rock burst control in panel 25110, as shown in Fig. 9 and Tables 1 and 2. All the boreholes were situated along the head gate in the coal body. From July 2010 to June 2011, more than 1870 boreholes for large diameter drilling were applied. And also, from July 2010 to August 2011, more than 170 boreholes for de-stress blasting were applied. In Tables 1 and 2, borehole parameters for large diameter drilling and de-stress blasting were optimized respectively.

It is seen from Fig. 9 that 363 m of gateway was damaged due to rock burst on 11 August 2010 while only 20 m of gateway was damaged due to rock burst on 1 March 2011. In Fig. 9(a), even the area with the application of large diameter drilling before parameter optimization (the pink ones) was damaged due to rock burst. While after parameter optimization, the area with the application of large diameter drilling (the red ones and the blue ones) was not damaged any more. Similarly in Fig. 9(b), only a small amount of boreholes were applied just prior to rock burst on 11 August 2010. While just before rock burst on 1 March 2011, a large amount of boreholes were applied. And this time, the area with the application of de-stress blasting was not damaged.

Fig. 10. Photographs of gateway damage taken after rock bursts occurring on (a) 11 August 2010, and (b) 1 March 2011.

Photographs of gateway damage due to the rock bursts are shown in Fig. 10. Burst energies of the bursts on 11 August 2010 and 1 March 2011 were 9×10^7 and 1.45×10^8 J, respectively. It is seen that the gateway damaged more seriously on 11 August 2010 even though the burst energy is smaller. Figs. 9 and 10 and Tables 1 and 2 clearly indicate that after the application of numerous boreholes and the optimization of parameters, the gateway damage induced by rock burst was significantly reduced, even though the burst energy was higher. Hence, it is concluded that large diameter drilling and de-stress blasting are suitable methods for FPIRB control.

6. Conclusions

In the case of normal mining, the roof strata fracture one by one, not simultaneously. When the coalface approaches the fault area, two or more roof strata fracture simultaneously in the fault area, leading to a rise in the dynamic and static stress in the pillar.

FPIRB, whose main factors of influence are fault slide induced dynamic stress and static stress in the pillar, can be subdivided into fault slide induced rock bursts, pillar failure induced rock bursts, and rock bursts induced by the interaction of both fault slides and pillar failure.

An analytic expression for the average static stress in the pillar has been obtained by solving the equations derived using a mechanical model of a fault–pillar and practical engineering calculation methods. The average static stress rises as the pillar width decreases and/or the roof fracture length increases. The stress is higher with a voussoir beam structure than it is without a voussoir beam structure. With a voussoir beam structure, stress is directly proportional to the squared length of the fractured roof and inversely proportional to the squared width of the pillar just before the roof block rotates. It is directly proportional to the roof fracture length and inversely proportional to the pillar width after rotation. When rotation occurs, there is a drop in the average static stress. Before rotation, the average static stress decreases according to the ratio of roof subsidence to thickness. In contrast, it is not affected by this ratio after rotation. In addition, the roof block rotates more readily at smaller pillar widths, larger roof thicknesses, and smaller roof subsidences.

The probability of FPIRB disasters can be reduced by lowering the static stress in the pillar and reducing the fault slide induced dynamic stress and energy accumulated in the pillar. Detailed methods to achieve this specifically include: pre-splitting the roof, filling the gob, making the coalface oblique to the fault, loosening and cracking the roof, controlling mining intensity, and loosening and cracking the coal mass. Practical experience shows that the effects of FPIRBs can be effectively mitigated by de-stress blasting and large diameter drilling.

Acknowledgments

This work was supported and financed by the National Natural Science Foundation of China and the Shenhua Group Corporation Limited (Project no. 51174285), the National Basic Research Program of China (No. 2010CB226805), the Research and Innovation Project for College Graduates of Jiangsu Province (No. CXZZ12_0949), and the Priority Academic Program Development of Jiangsu Higher Education Institutions (No. SZBF2011-6-B35).

References

[1] Dou LM, He XQ. Theory and Technology of Rock Burst Prevention. Xuzhou: China University of Mining and Technology Press; 2001; 1–45 (in Chinese).
[2] Qian MG, Shi PW. Mine Pressure and Ground Control. Xuzhou: China University of Mining and Technology Press; 2003; 65–97 (in Chinese).
[3] Cao AY, Dou LM, Yan RL, Jiang H, Lu CP, Du TT, et al. Classification of microseismic events in high stress zone. Min. Sci. Technol. 2009;19:718–23.
[4] Chen XH, Li WQ, Yan XY. Analysis on rock burst danger when fully-mechanized caving coal face passed fault with deep mining. Safety Sci. 2012;50:645–8.
[5] Cianciara A, Cianciara B. Method of predicting tremors on the basis of seismic emission registered in exploitation workings. Tectonophysics 2008;456:62–6.
[6] Díaz Aguado MB, González C. Influence of the stress state in a coal bump-prone deep coalbed: a case study. Int. J. Rock Mech. Min. Sci. 2009;46:333–45.
[7] Gaviglio P. A fault and stress field analysis in a coal mine (Gardanne, Bouches Du Rhone, France). Tectonophysics 1985;113:349–66.
[8] Dehghan S, Shahriar K, Maarefvand P, Goshtasbi K. 3-D modeling of rock burst in pillar No. 19 of Fetr6 chromite mine. Int. J. Min. Sci. Technol. 2013;23:231–6.
[9] Dou LM, He XQ. Model for rock burst failure and its critical values of acoustic and electromagnetic emission. J. China Univ. Min. Technol. 2004;33:504–8 (in Chinese).
[10] Li ZH, Dou LM, Lu CP, Mu ZL, Cao AY. Study on fault induced rock bursts. J. China Univ. Min. Technol. 2008;18:321–6 (in Chinese).
[11] Li ZL, Dou LM, Cai W, He J, Wang GF, Liu J, et al. Fault–pillar induced rock burst mechanism of thick coal seam in deep mining. Chin. J. Rock Mech. Eng. 2013;32:333–42 (in Chinese).
[12] Pan Y, Li AW, Qi YS. Fold catastrophe model of dynamic pillar failure in asymmetric mining. Min. Sci. Technol. 2009;19:49–57.
[13] Patynska R, Kabiesz J. Scale of seismic and rock burst hazard in the Silesian companies in Poland. Min. Sci. Technol. 2009;19:604–8.
[14] Stewart RA, Reimold WU, Charlesworth EG, Ortlepp WD. The nature of a deformation zone and fault rock related to a recent rockburst at Western Deep Levels Gold Mine, Witwatersrand Basin, South Africa. Tectonophysics 2001;337:173–90.
[15] Wang HW, Jiang YD, Zhu J, Shan RY, Wang C. Numerical investigation on the assessment and mitigation of coal bump in an island longwall panel. Int. J. Min. Sci. Technol. 2013;23:625–30.
[16] Sainoki A, Mitri HS. Dynamic behaviour of mining-induced fault slip. Int. J. Rock Mech. Min. Sci. 2014;66:19–29.
[17] He J, Dou LM, Cao AY, Gong SY, Lu JW. Rock burst induced by roof breakage and its prevention. J. Central South Univ. Technol. 2012;19:1086–91.
[18] Cao AY, Dou LM, Li FC, Jiang H, Qu Y, Han RJ. Study on characteristic of overburden movement in unsymmetrical isolated longwall mining using microseismic technique. Proced. Eng. 2011;26:1253–62.
[19] Mu ZL, Dou LM, He H, Fan J. F-structure model of overlying strata for dynamic disaster prevention in coal mine. Int. J. Min. Sci. Technol. 2013;23:513–9.
[20] Qian MG. A structural model of overlying strata in longwall workings and its application. J. China Inst. Min. Technol. 1982:1–11, (in Chinese).
[21] Qian MG. Conditions required for Equilibrium of overlying strata at working areas. J. China Inst. Min. Technol. 1981:31–40, (in Chinese).
[22] Diederichs MS, Kaiser PK. Stability of large excavations in laminated hard rock masses: the voussoir analogue revisited. Int. J. Rock Mech. Min. Sci. 1999;36:97–117.
[23] Sofianos AI. Analysis and design of an underground hard rock voussoir beam roof. Int. J. Rock Mech. Min. Sci. 1996;33:153–66.
[24] Ju JF, Xu JL. Structural characteristics of key strata and strata behaviour of a fully mechanized longwall face with 7.0 m height chocks. Int. J. Rock Mech. Min. Sci. 2013;58:46–54.
[25] Brady BHG, Brown ET. Excavation design in stratified rock. Rock Mechanics for Underground Mining. 3rd ed.. Dordrecht: Kluwer; 2004; 224–41.
[26] Fan J, Dou LM, He H, Du TT, Zhang SB, Gui B, et al. Directional hydraulic fracturing to control hard-roof rockburst in coal mines. Int. J. Min. Sci. Tech 2012;22:177–81.
[27] Feng XJ, Wang EY, Shen RX, Wei MY, Chen Y, Cao XQ. The dynamic impact of rock burst induced by the fracture of the thick and hard key stratum. Proced. Eng. 2011;26:457–65.
[28] Mu ZL, Dou LM, Ni XH, Zhang MW. Research on the influence of roof strata on rock burst risk. J. China Univ. Min. Technol 2010;39:40–4 (in Chinese).
[29] Xu NW, Tang CA, Li LC, Zhou Z, Sha C, Liang ZZ, et al. Microseismic monitoring and stability analysis of the left bank slope in Jinping first stage hydropower station in southwestern China. Int. J. Rock Mech. Min. Sci. 2011;48:950–63.
[30] Jiang QA, Feng XT, Xiang TB, Su GS. Rockburst characteristics and numerical simulation based on a new energy index: a case study of a tunnel at 2500 m depth. Bull. Eng. Geol. Environ. 2010;69:381–8.